IEEE Access
Multidisciplinary ⋮ Rapid Review ⋮ Open Access Journal

Received March 11, 2022, accepted March 21, 2022, date of publication March 31, 2022, date of current version April 8, 2022.

Digital Object Identifier 10.1109/ACCESS.2022.3163850

Ultrawideband RCS Reduction of Planar and Conformal Surfaces Using Ultrathin Polarization Conversion Metasurface

JOYSMITA CHATTERJEE[1], (Graduate Student Member, IEEE), AKHILESH MOHAN[2], (Member, IEEE), AND VIVEK DIXIT[1], (Member, IEEE)

[1]Department of Electronics and Electrical Communication Engineering, Indian Institute of Technology Kharagpur, Kharagpur, West Bengal 721302, India
[2]Department of Electronics and Communication Engineering, Indian Institute of Technology Roorkee, Roorkee, Uttarakhand 247667, India

Corresponding author: Joysmita Chatterjee (joysmita.chatterjee@gmail.com)

ABSTRACT A metasurface-based polarization converter for ultrawideband radar cross-section (RCS) reduction of planar and conformal surfaces is presented in this paper. Initially, a polarization converter is designed which consists of a modified concentric double (MCD) square ring resonator-based unit cell along with an air gap in between the substrate and the ground plane. This air gap enhances the polarization conversion bandwidth (PCBW) of the converter. An ultrawide PCBW ranging from 6.3 – 20.5 GHz (106%) is obtained with a high polarization conversion ratio (PCR) of 0.9 for normal incident EM waves. The conversion efficiency is also found to be stable for oblique incidences over the aforementioned band with a PCR of above 0.8 upto ±35° angles of incidence. Later on, a checkerboard configuration of the polarization conversion metasurface (PCMS) array and its mirror array is applied on a planar as well as on a cylindrical conformal surface for reducing the radar cross section (RCS). It is observed that a consistent 10 - dB co-polarized monostatic RCS reduction is achieved with the planar PCMS surface over an ultrawideband (5.5 – 20.5 GHz). Even with the cylindrical surface, nearly 10 dB RCS reduction is obtained upto central angles of 60° over a wideband. Both the structures are simulated and measured after fabrication, and a reasonably good agreement is obtained between them.

INDEX TERMS Artificial magnetic conductor (AMC), conformal checkerboard surface, polarization converter (PC), radar cross section (RCS), ultrawideband.

I. INTRODUCTION

Polarization convertersform an integral part of modern wireless communication, due to their extensive range of applications in circularly polarized antennas [1], liquid crystal displays, and radar cross section (RCS) reduction [2]. Polarization conversion can be achieved through traditional techniques, such as the use of birefringence wave plates [3], liquid crystals [4], Faraday effects [5], etc. However, these techniques have some drawbacks of large thickness and narrow bandwidth that limit its practical applications.

In the present scenario, metasurfaces (MSs), which are the planar equivalent of metamaterials, are being employed to improve the performance of antennas and wireless communication systems [6]–[9]. They are also being utilized to achieve polarization conversion for various applications. The converters designed using MSs are generally low profile and lightweight in nature. Various reflection and transmission type polarization converters are designed which involves the anisotropic nature of the MS [10]–[25]. Reflection type converters consist of structures like double head arrow [10], cut wires [11], [12], V-shaped resonators [13], [14], and resonators loaded with vias along the diagonal [15], [16] to name a few. Some of these reported works have high polarization conversion efficiencies (PCE), but they are limited in their polarization conversion bandwidths (PCBWs), which inhibits their practical usage in imaging and sensing applications that require a wide bandwidth. Therefore, the need arises of designing the MS-based polarization converters with ultra-wide bandwidth, which has been accomplished by few researchers. Various techniques have been adopted to increase the PCBW like stacking multiple layers [17], [23],

The associate editor coordinating the review of this manuscript and approving it for publication was Shah Nawaz Burokur.

optimizing the unit cells to generate multiple plasmon resonances [13], [24], and also by using two different types of AMC unit cells [25].

Another important aspect is the stability of the converter to oblique incident EM waves which affect its use in conformal structures. This aspect finds immense significance in several microwave and wireless communication applications where surfaces are curved like radomes, ships, aircraft, missiles, and various transmitters. This is due to the fact that the behavior of polarization conversion metasurface (PCMS) depends extensively on the curvature of surfaces, as the angle of incidence of the electromagnetic waves changes according to the surface curvature. In most of the planar works [10]–[25], it is observed that even if ultrawide PCBW is obtained with a high PCE (>80%), the PCE value remains stable only for normal incidence. To overcome this problem, researchers conceived the idea that incidence angle insensitivity occurs if the substrates used are ultrathin. However, the use of ultrathin substrates also reduces the operating bandwidth. In [26], researchers designed an electrically thin converter, where the PCE is unaffected by the variations in the incidence angles. However, the fractional polarization conversion bandwidth is only 73% (5 – 10.8 GHz) and the PCE value in the lower frequency range is less than 70%. Therefore, a tradeoff is required amongst polarization conversion bandwidth, incidence angle insensitivity, and thickness of the substrate. The design of an ultrathin polarization converter with a high PCR value (> 0.9) over an ultrawide frequency band along with angular stability is in great demand and is also a challenging task.

One of the key applications of polarization converters is RCS reduction of antennas and surfaces. By phase cancellation technique from a checkerboard arrangement of the (PCMS) array and its mirror array, a wideband RCS reduction can be obtained. The RCS reduction bandwidth can be suitably varied by properly adjusting the dimensions of a single element to enhance the PCR and PCBW. Various works have been reported in the literature that employs the above concept to achieve wideband RCS reduction of planar surfaces and antennas [2], [28]–[30]. The PCMS reported in [2], which is a chessboard configuration of a fishbone-shaped element and its mirror image, leads to the RCS reduction of a slot antenna over a bandwidth of 100%. Similarly, the radar cross section of a patch antenna presented in [28] gets reduced by a shared aperture metasurface over a bandwidth of 61.5% (9 – 17 GHz). An ultrawideband polarization rotation reflective surface (PRRS) is designed in [29] which consists of square and L-shaped patches. This PRRS is developed into a checkerboard configuration that reduces the RCS of a planar metallic sheet over an ultrawideband of 98%. All the aforementioned works aim to reduce the RCS of planar structures and surfaces.

As stated previously, for several microwave and wireless communication systems such as radomes, ships, aircraft, missiles, etc where the surfaces are conformal, there is a requirement to reduce the RCS of these structures for stealth applications. However, very few works aiming at the reduction of the RCS of conformal structures using a checkerboard configuration are reported. The letter, in [31], is the first and only instance where checkerboard design architectures have been applied on curved structures and their impact on RCS reduction has been investigated. Nevertheless, there are certain drawbacks to these structures. Firstly, it uses two different types of AMC unit cells to increase the bandwidth that leads to design complexity. Besides that, only 5 dB RCS reduction is obtained over a bandwidth of 7 - 9 GHz for two different radii of curvatures. These problems have been addressed in the proposed work.

In this work, the polarization converter-based approach has been used to eradicate the design complexities and achieve wideband RCS reduction in the boresight direction through the phase cancellation technique. A checkerboard configuration is formed consisting of the PCMS array along with its mirror array and applied on planar as well as cylindrically curved surfaces. To the best of the authors' knowledge, this is the first instance where a checkerboard configuration of a single AMC-based PCMS array and its mirror image are used for RCS reduction of conformal surfaces over an ultrawide bandwidth. Comparisons have also been drawn between the simulated results for various radii of curvature of the cylindrical surfaces. The structure is well suited to be applied for stealth applications in military systems operating in X-, Ku-, and parts of C- and K – bands.

This paper is organized into different sections. Section II presents a study of the polarization converter including its stability against obliquely incident waves. Section III investigates the impact of the checkerboard surface on the radar cross section reduction of planar as well as curved surfaces. Section IV presents the experimental results of the fabricated structures and a comparison with the simulated results as well. Finally, conclusions are drawn in section V.

II. CONVERTER DESIGN AND ANALYSIS

A. PROPOSED POLARIZATION CONVERTER DESIGN

Figure. 1 shows the proposed modified concentric double (MCD) square ring resonator-based unit cell which acts as the polarization converter. It consists of two concentric square rings of different widths. To introduce anisotropy, the corners along the diagonal axis (AA′) have been truncated as shown in the figure. Furthermore, an L-shaped strip is added to the inner resonator to generate an additional resonance. The unit cell is printed on Rogers RT/duroid 5880 substrate ($\varepsilon_r = 2.2$ and $\tan\delta = 0.0009$) of an ultrathin thickness of height h to enable it to be suitably bent for conformal applications. An air layer of height h_{air} is sandwiched between the ground plane (realized by a copper sheet) and the substrate as shown in Figure. 1 (a). This is primarily done to enhance the polarization conversion bandwidth (will be discussed later on). This combination of MCD square ring resonator alongwith the air layer sandwiched between the substrate and the ground plane forms the polarization converter. The dimensions of the converter are detailed in Figure. 1. All

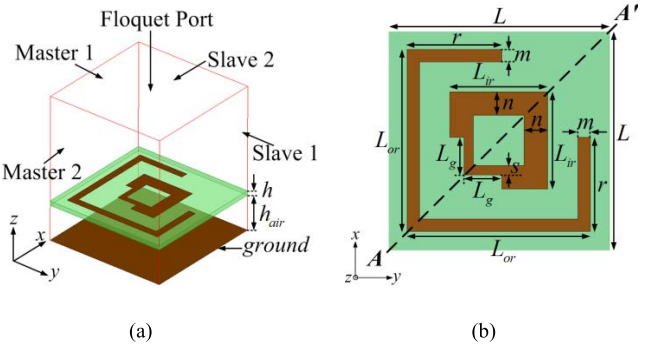

FIGURE 1. Proposed ground backed MCD square ring resonator based polarization converter. (a) Isometric view and simulation setup (b) Top view. Dimensions are: $L = 7$, $L_{or} = 5.8$, $r = 3$, $m = 0.4$, $L_{ir} = 3.1$, $L_g = 1.2$, $s = 0.3$, $n = 0.75$, $h_{air} = 3.5$, and $h = 0.508$. All dimensions are in mm.

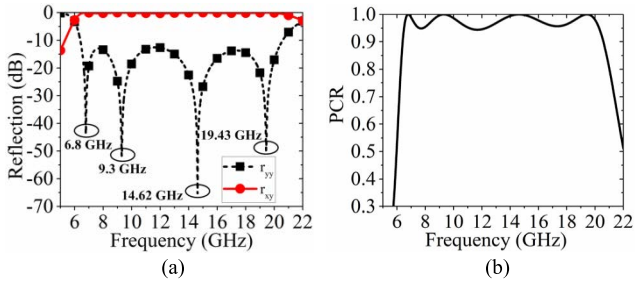

FIGURE 2. (a) Simulated co– and cross-polarized reflection coefficients of the proposed converter (b) Polarization conversion ratio (PCR).

the simulations have been conducted in Ansys HFSS EM simulation software.

The polarization conversion property is studied by allowing a y-polarized plane wave to impinge on the converter. The simulation setup is shown in Figure. 1(a). Due to the anisotropic nature of the structure (along AA′), the reflected wave consists of both co-and cross-polarized components. These components are given by,

$$r_{yy} = |E_{yr}| / |E_{yi}| \quad (1)$$

$$r_{xy} = |E_{xr}| / |E_{yi}| \quad (2)$$

where r_{yy} and r_{xy} are the co- and cross-polarized components respectively, and the polarization conversion ratio (PCR) and the polarization conversion efficiency (PCE) are given by

$$PCR = r_{xy}^2/(r_{xy}^2 + r_{yy}^2) \quad (3)$$

$$PCE = PCR \times 100\% \quad (4)$$

Figure. 2 (a) shows the co- and cross-polarized reflection responses from the converter with a Floquet port excitation. The calculated polarization conversion ratio is plotted in Figure. 2(b). It is observed that the value of PCR is greater than 0.9 over the entire frequency band from 6.3 – 20.5 GHz and rises to 1 at four distinct frequencies of 6.8, 9.3, 14.62, and 19.43 GHz. This indicates that the total energy of the y-polarized incident wave is completely converted to x-polarized reflected wave. Due to the diagonal symmetry of the unit cell along AA′, similar results would be obtained for the x-polarized incident wave.

B. EVOLUTION OF THE POLARIZATION CONVERTER

While designing the MCD square ring resonator-based polarization converter, two aspects have been taken into consideration. Firstly, we have targeted the entire X- and Ku- bands and also parts of C- and K-bands since these frequency bands are mostly suited for radar applications. Secondly, the geometry of the unit cell is designed and optimized to obtain an ultrawide polarization conversion bandwidth with a very high PCE (>90%).

To begin with, initially two concentric square rings of different widths printed on the substrate are chosen as the unit cell as shown in Figure. 3 (a) (unit cell#1). No air gap between the ground plane and the dielectric substrate is considered at this stage. Since the structure is not anisotropic, only co-polarized components are predominant, and the magnitude of PCR is very low (≈ 0) which is quite obvious [Figure. 3 (e)]. To introduce anisotropy and generate both co- and cross-polarized components, the corners of the resonators are truncated and unit cell#2 evolves [Figure. 3 (b)]. The truncation on the inner resonator is L-shaped and that on the outer resonator is inverted L-shaped, and they are placed on opposite corners as shown in the figure. This is done so that, along a particular direction every ring resonator has a truncated side as well as a non-truncated side, causing an x- or a y – polarized incident wave to allow the flow of current not only in the direction of polarization but also in the perpendicular direction. These currents along the truncated and non-truncated sides have a phase difference, which gives rise to cross-polarization conversion [26]. As seen from Figure. 3 (e), due to the newly introduced asymmetry in the converter, the y-polarized incident wave gets reflected along the x-direction, with 100% PCE at four distinct frequencies of 6.95, 13.03, 17.27, and 21.5 GHz. However, the PCBW [frequency ranges over which mag (PCR) > 0.9] is very narrow for each band.

To increase the bandwidth, an air layer is sandwiched between the copper sheet (acting as the ground plane) and the substrate (unit cell #3) [Figure. 3(c)]. This air gap acts as a low permittivity substrate and thus aids in increasing the polarization conversion bandwidth of the converter [32]. The thickness of the air gap (h_{air}) is optimized to achieve the highest bandwidth by merging the resonant frequencies or bringing them closer. This process is very effective since it increases the PCBW without increasing the lateral dimensions of the structure. The PCBW, in this case, is 77% (6.26 – 14.16 GHz) with a high PCR of 0.9.

The frequencies at which the PCR magnitude rises to 1 are 6.6, 9, and 12.6 GHz. To further increase the bandwidth, a narrow L-shaped strip is added to the truncated corner of the inner resonator which results in the proposed unit cell [Figure. 3(d)]. Due to the addition of this L-shaped strip, mutual coupling occurs between the inner and outer resonators, and the third resonant frequency at 12.6 GHz shifts to 14.62 GHz, and an additional resonance is generated at 19.43 GHz. Owing to the multiple plasmon resonances being generated; the polarization converter produces an

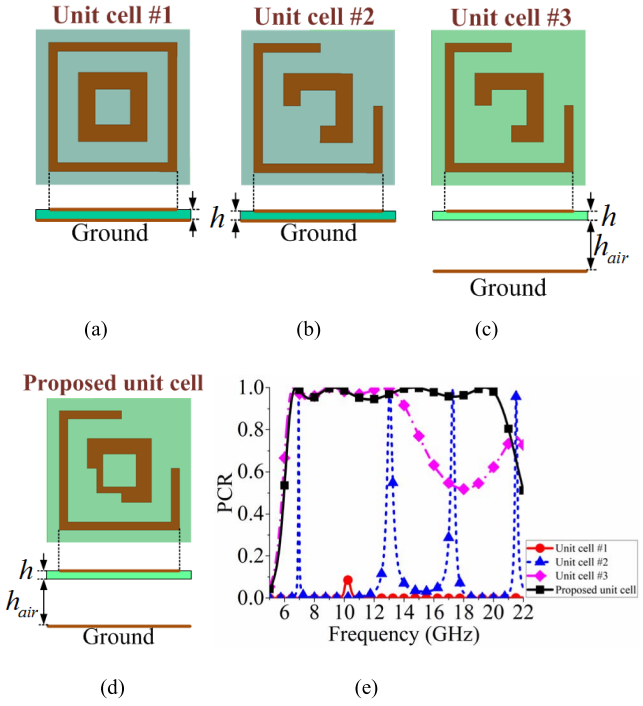

FIGURE 3. Study of different configurations of the polarization converter (a) unit cell #1 (b) unit cell #2 (c) unit cell #3 (d) proposed unit cell and (e) their corresponding PCR values.

ultrawide PCBW of 106% (6.3 – 20.5 GHz) with a high PCR magnitude of 0.9.

C. CURRENT DISTRIBUTION AND ANALYSIS OF THE RESONANT FREQUENCIES

To get a better physical insight, surface current distributions at the four resonant frequencies (frequencies at which polarization conversion ratio is nearly 100%) of 6.8, 9.3, 14.62, and 19.43 GHz are plotted in Figure. 4. At each of these resonant frequencies, plasmon resonances are generated by the electric and magnetic responses of the proposed converter [13]. The black arrows denote the resultant current direction on the top unit cell and bottom ground plane. At the lowest resonant frequency of 6.8 GHz [Figure. 4 (a)], it can be observed that surface current mainly concentrates on the outer ring and also changes directions at the corners which make the outer ring behave as an electric dipole [11]. Generally, the surface currents on the top unit cell at each of the resonant frequencies produce induced currents on the ground plane. The direction of the induced currents determines the type of resonance. If the surface currents on the top metallic unit cell are parallel to those induced on the ground plane, an electric resonance is generated whereas if the surface currents on the top unit cell and induced currents on the bottom ground plane are anti-parallel to each other, forming loops of currents, magnetic resonances are generated [13]. As observed in Figure. 4 (a), magnetic resonance is generated at the lowest resonant frequency of 6.8 GHz due to the circulating current flow. Figure. 4 (b) depicts the current distribution at the second resonant frequency of 9.3 GHz.

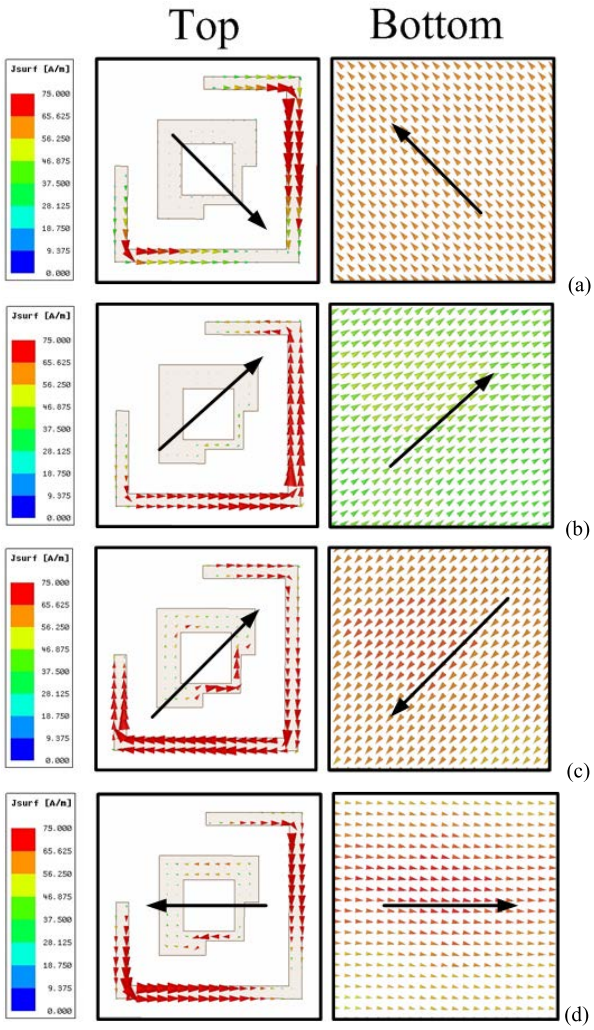

FIGURE 4. Surface current distributions on the unit cell (top layer) and ground plane (bottom layer) at four resonant frequencies (a) 6.8 GHz, (b) 9.3 GHz, (c) 14.62 GHz, and (d) 19.43 GHz. The black arrows indicate the resultant surface current direction.

Similar to the first case; current mainly concentrates on the outer ring. It is also observed that the current on the outer ring does not change directions causing it to behave as a cut-wire resonator [33]. Moreover, the resultant currents on the top layer are parallel to the induced currents on the bottom ground plane generating electric resonance. In the case of the higher resonant frequencies in Figure. 4 (c) and (d), it is observed that the currents are distributed on both the inner and outer resonators. Current flows continuously for the third resonant frequency, and in opposite directions for the fourth resonant frequency of 19.43 GHz, causing the resonator to behave as cut-wire and electric dipole respectively. In the case of the third resonance at 14.62 GHz, different resonant cases are perceived. The current flows in opposite directions on both the inner and outer resonators. The resultant currents on the inner resonator and bottom ground plane are antiparallel to each other generating magnetic resonance, whereas, the currents on the outer resonator and the bottom layer are parallel to each other generating electric resonance. A similar

TABLE 1. Analysis of the resonant frequencies from the current distribution of Figure. 4.

Resonant Frequency	Behavior of the Converter	Type of Resonance
6.8 GHz	Electric Dipole	Magnetic
9.3 GHz	Cut-wire Resonator	Electric
14.62 GHz	Cut-wire Resonator	Magnetic + Electric
19.43 GHz	Electric Dipole	Magnetic + Electric

situation is also observed in the case of the fourth resonant frequency [Figure. 4 (d)], where both electric and magnetic resonances are excited for the outer and inner resonators respectively. Therefore, it can be concluded that the first and second resonant frequencies are purely due to magnetic and electric resonance between the outer resonator and ground plane, respectively. Whereas, the third and fourth resonant frequencies are due to the combination of both electric and magnetic resonances between the inner and outer resonators and the ground plane. This is also briefed in Table 1. Due to the excitation of multiple plasmon resonances; an ultrawide PCBW (106%) is obtained.

D. INSENSITIVITY TO OBLIQUE INCIDENCE

It is known that polarization converters can be applied for the RCS reduction of planar surfaces or antennas. In order to apply them for the RCS reduction of conformal surfaces, their performance in terms of polarization conversion bandwidth and polarization conversion efficiency should be stable against various incidence angles. It has been reported in the literature that unit cells offer incidence angle invariance behavior if they are designed on ultrathin substrates or the dielectric constant of the substrate is high [26]. However, this causes a remarkable reduction in the polarization conversion bandwidth. So, there should be a tradeoff between the polarization conversion bandwidth, angular stability, and substrate thickness. The key to achieving a wider bandwidth, with an ultrathin substrate, is to carefully design the polarization converter to obtain multiple plasmon resonances which can increase the PCBW. Figures. 5 (a) and (b) shows the co- and cross-polarized reflections for different angles of y – polarized incident waves on the proposed converter. It is observed that, due to the ultrathin thickness of the substrate [$(h + h_{air}) \ll \lambda_L$)], and small size of the unit cell (0.15 λ_L, where λ_L is the wavelength corresponding to the lowest operating frequency of 6.3 GHz.), both the co- and cross polarized reflections are stable against incident angle variations, Figure. 5(c) depicts the variation of PCR with respect to frequency for various angles of y – polarized incidence. It is observed that the PCBW and PCR values are stable and well preserved for angles of incidence upto ±35°. A minor degradation is observed around 8 GHz for 35° incident angle. However, the PCR values are still greater

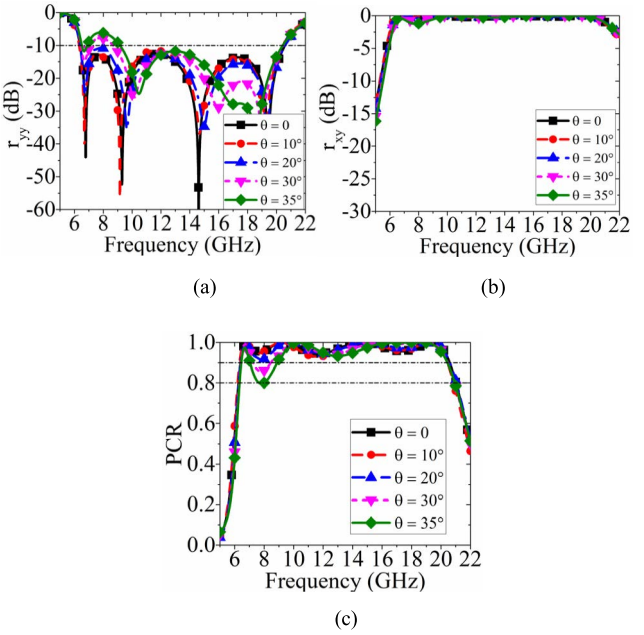

FIGURE 5. Response of the PCMS unit cell to various angles of incidence of y-polarized plane wave in respect of (a) co-polarization reflection (r_{yy}), (b) cross-polarization reflection (r_{xy}), and (c) PCR.

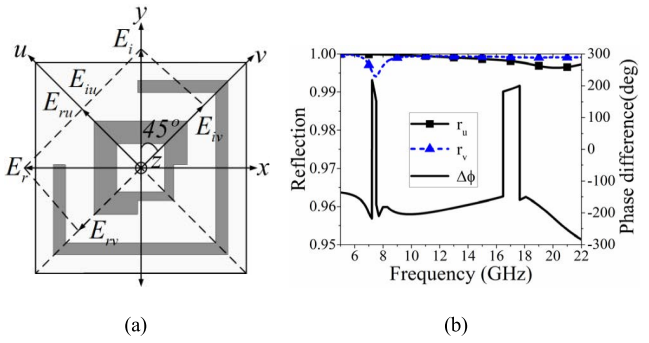

FIGURE 6. (a) Polarization conversion mechanism of a normal incident y-polarized wave on the designed polarization converter (b) Reflected amplitude and phase difference between u- and v-polarized waves.

than 80% over the entire bandwidth which is reasonably good. With further increase in the angles of incidence, the performance degrades due to the small size of the unit cell and also due to the increase in the propagation phase of the EM waves compared to normal incidence leading to destructive interference on the MS [11]. Since the structure is symmetric along AA′, similar results would be obtained for x-polarized incidence and are therefore not shown.

E. THEORETICAL ANALYSIS OF POLARIZATION CONVERSION

To gain a better understanding of the polarization conversion mechanism, a theoretical basis is developed. As seen in Figure. 6, the MCD square ring resonator-based polarization converter possesses anisotropy along u- and v-

axis. Let us consider a y-polarized incident wave. It can be decomposed into two orthogonal u- and v- components whose

magnitudes are exactly equal to 1. The incident wave $\vec{E}_i$ can be represented as,

$$\vec{E}_i = \hat{y}E_{yi} = \hat{u}E_{iu} + \hat{v}E_{iv} = E_{yi}cos(45^\circ)(\hat{u} + \hat{v}) \quad (5)$$

where E_{yi} can be represented in space-time co-ordinates as $\vec{E}_{yi}(z,t) = \hat{y}E_{yi}e^{j(wt-kz)}$. Similarly, the reflected wave can also be expressed as,

$$\vec{E}_r = \hat{u}E_{ru} + \hat{v}E_{rv} = \hat{u}r_uE_{iu} + \hat{v}r_vE_{iv} = E_{yi}cos(45^\circ)\left(r_u\hat{u} + r_v\hat{v}\right) \quad (6)$$

where $\hat{y}$, $\hat{u}$, and $\hat{v}$ denote the unit vectors along the y, u, and v axis, r_u and r_v denote the complex reflection coefficients for u- and v-polarized incident waves respectively. Since Rogers RT/duroid 5880 substrate has a very negligible dielectric loss tangent (0.0009), therefore, both the reflection coefficients have unity magnitude [20]. It is observed that, even though the incident field is y-polarized, the reflected field is directed along both x- and y-directions due to the anisotropic nature of the unit cell. Let the reflection phase of u- and v-polarized waves be ϕ_u and ϕ_v respectively. Thus, from equations (5) and (6), the reflected field can be re-written as,

$$\vec{E}_r = E_{yi}cos(45^\circ)[r_ue^{j(wt-kz+\phi_u)}\hat{u} + r_ve^{j(wt-kz+\phi_v)}\hat{v}] \quad (7)$$

Comparing equations (6) and (3), the u- and v components can be expressed as,

$$E_{ru} = r_uE_{yi}cos(45^\circ)cos(wt - kz + \phi_u) \quad (8a)$$

$$E_{rv} = r_vE_{yi}cos(45^\circ)cos(wt - kz + \phi_v) \quad (8b)$$

With reference to the detailed analysis presented in [24], the co- and cross-polarized reflections, r_{yy} and r_{xy} are given as,

$$r_{yy} = \frac{|E_{yr}|}{|E_{yi}|} = \sqrt{(1 + cos\Delta\phi)/2} \quad (9a)$$

$$r_{xy} = \frac{|E_{xr}|}{|E_{yi}|} = \sqrt{(1 - cos\Delta\phi)/2} \quad (9b)$$

If $\Delta\phi = \pm 180^\circ$, $r_{yy} = 0$ and $r_{xy} = 1$, and so a 90° polarization conversion is obtained. The amplitudes of u- and v – polarized waves and the phase difference between them are shown in Figure. 6 (b). It is observed from the figure that the amplitudes are almost the same and nearly equal to 1, while the phase difference is nearly 180° from 6.3 – 20.5 GHz depicting complete polarization conversion for the above band of operation.

F. PARAMETRIC ANALYSIS OF THE POLARIZATION CONVERTER

Structural parametric analyses are carried out to reveal the geometrical effects of the converter on the polarization conversion ratio (PCR) and also to obtain the optimized design parameters. When one of the parameters is optimized, all others are kept constant.

Firstly, the effects of the width of the outer square ring (m) on the PCR performance of the polarization converter are studied. It is observed from Figure. 7 (a), with an increase in the width of the outer square ring, the PCR bandwidth increases. This is due to a shift in the highest resonant frequency that leads to increased bandwidth. However, when the value of m changes from 0.4 mm to 0.65 mm, the PCR performance deteriorates at the higher frequency band. The value of PCR falls below 0.8 at some portions of the upper frequency band. Hence, $m = 0.4$ is chosen as an optimized design parameter value.

The side length of the inner square ring (L_{ir}) of the converter also plays a major role in the PCR performance. The PCR bandwidth is high for lower values of L_{ir} and reduces when the value increases from 2.7 to 3.5 mm. Furthermore, the PCR performance gets affected at both lower and upper bands for lower values of L_{ir}. For the value of $L_{ir} = 3.5$ mm, the PCR performance gets affected at the upper band, with the PCR value falling below 0.9. Considering all these aspects, the optimized value of L_{ir} is chosen to be 3.1 mm, which not only gives a good PCR performance but also provides a wide PCR bandwidth. This is clearly depicted in Figure. 7 (b).

The PCR performance of the converter is also affected by the changes in the truncation length of the outer square ring resonator. Modifications in the truncation length produce changes in the values of 'r' which affects the PCR performance of the converter. With the increase in the value of r (reduction in truncation length), the PCR bandwidth increases. However, the conversion efficiency reduces below 85% at the upper frequency bands. This is evident from Figure. 7 (c). So, $r = 3$ mm is chosen as an optimized design parameter value.

The width of the L-shaped strip (s) added to the inner resonator also contributes to the PCR bandwidth of the converter. As observed in Figure. 7 (d), in the absence of the strip, the fourth resonance is not being generated, and the PCRBW ranges from 6.3 – 13.8 GHz (75%). On addition of the L-shaped strip, mutual coupling occurs between the inner and outer resonators resulting in the shifting of the third resonant frequency from 12.6 GHz to 14.62. Also, an additional resonance is generated at 19.43 GHz. However, as evident from the figure, with further increase in strip width, not only the PCRBW reduces, the PCR value reduces below 0.9 at the lower bands. Thus, the value of s is chosen as 0.3 mm to maintain a wide PCRBW with a high PCR value. Based on the above parametric analysis, the optimized dimensions of the converter are provided in Figure. 1.

G. COMPARISON OF THE PROPOSED CONVERTER WITH OTHER WIDEBAND CONVERTERS IN LITERATURE

Table 2 presents a comparison of the proposed polarization converter with other wideband converters. It can be seen that the proposed converter is not only ultrathin but also has a wide PCBW compared to others reported in the literature. Even though the converter in [26] shows an incidence angle insensitive behavior, yet it has a limited PCBW. The converter in [23] has a high PCBW but nothing has been reported about its performance for oblique incident waves. On the other hand, the proposed MCD square ring resonator-based

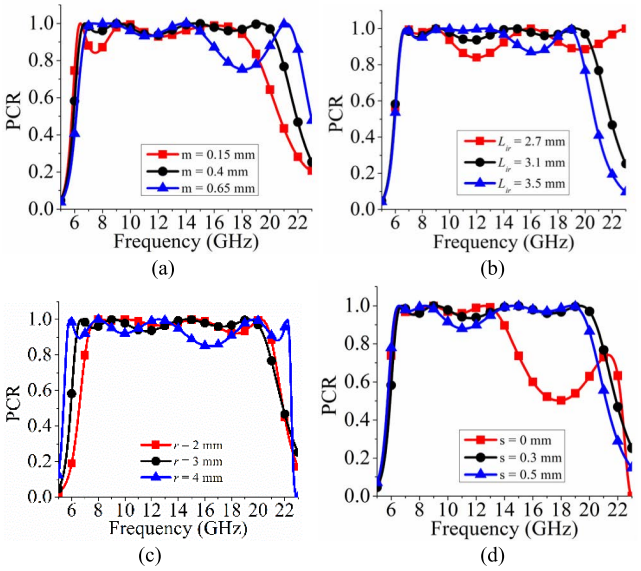

FIGURE 7. Simulated PCR for different values of (a) *m* (b) L_{ir} (c) *r*, and (d) *s*.

polarization converter not only has an ultrawide PCBW of 106% but also shows insensitivity to oblique incidence at least up to ±35° incidence angles.

III. DESIGN OF THE POLARIZATION CONVERSION METASURFACE AND ITS APPLICATION IN RCS REDUCTION

In this section, the MCD square ring resonator-based polarization converter is applied for RCS reduction of planar and conformal surfaces. To accomplish this, a checkerboard configuration consisting of an array of the converter and its mirror image is developed. RCS reduction follows the principle of reflective wave cancellation in the boresight direction. This can be realized if the cross polarized reflection phase difference between the polarization converter and its mirror image are tuned to lie within 180° ± 37° [31]. This mechanism is vividly illustrated in Figure. 8. It can be observed that the reflected E-field in the case of the proposed unit cell is along the x-direction (mechanism explained in Section II), whereas it is along the +x direction for its mirror image. Thus, both the reflected waves have a 180° phase difference between them, producing a null in the boresight direction. Figure. 8(c) depicts the cross-polarized reflection phase difference between the unit cell and its mirror image. It is seen that a consistent 180° ± 4° phase difference is maintained over an ultrawideband of 5 – 22 GHz. It will be shown later, that checkerboard architecture can facilitate scattering of most of the reflected energy in different undesired directions, thereby leading to RCS reduction in the boresight direction.

A. RCS REDUCTION OF A PLANAR METALLIC SHEET

In this sub-section, we discuss how the polarization converter can be applied for the RCS reduction of a planar metallic sheet. To accomplish this, a supercell is designed which

TABLE 2. Comparison of the proposed polarization converter with other reported wideband converters.

Ref.	Substrate thickness , mm	Polarizer Thickness, Mm	Operating PCBW (GHz)	Relative PCBW (%)	Sensitivity to oblique incidence
[11]	1.6	1.6	12.4 – 27.96	77	Yes
[23]	4	4	7.8 – 34.7	126.6	N.M.
[24]	2.8	2.8	6.99 – 9.18, 11.66 – 20.4	27, 54.5	N.M.
[26]	2.4	2.4	5 – 10.8	73.4	Insensitive upto ±45°
[27]	3	3	4.2 – 5.5 , 9 – 14	26.8, 43.5	N.M.
[30]	2	4	6.03 – 17.78	98	Yes
This Work	4	4	6.3 – 20.5	106	Insensitive upto ±35°

N.M.: Not Mentioned,

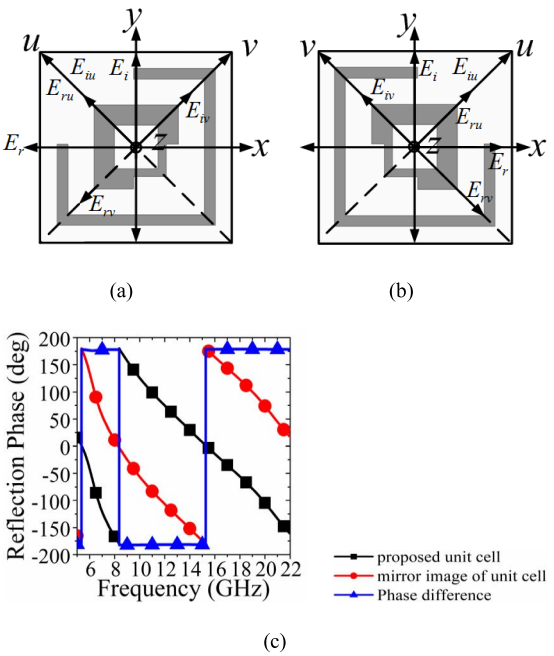

FIGURE 8. Polarization conversion technique of a normal incident y-polarized plane wave by the (a) proposed converter and its (b) mirror image (c) Cross polarization reflection phase of the unit cell, mirror unit, and the phase difference between them.

consists of a checkerboard configuration comprising of the PCMS array and its mirror image arranged into four quadrants each of which consists of 5 × 5 MCD square ring resonator-based unit cells [Figure. 9 (a)]. The total size of the structure is 78 mm × 78 mm × 4 mm ($1.64\lambda_L \times 1.64\lambda_L \times 0.08\lambda_L$, λ_L being measured at the lowest operating frequency of 6.3 GHz). The PCMS array and its mirror image produce a 90° and −90° phase shift to the reflective cross-polarized waves, thus cancelling it out and giving rise to RCS reduction in the boresight direction. The supercell is further replicated and arranged into four quadrants to produce a large PCMS surface, consisting of a 2 × 2 arrangement of the checkerboard configuration [Figure. 9(b)]. The lateral dimensions of the entire surface are 156 mm × 156 mm.

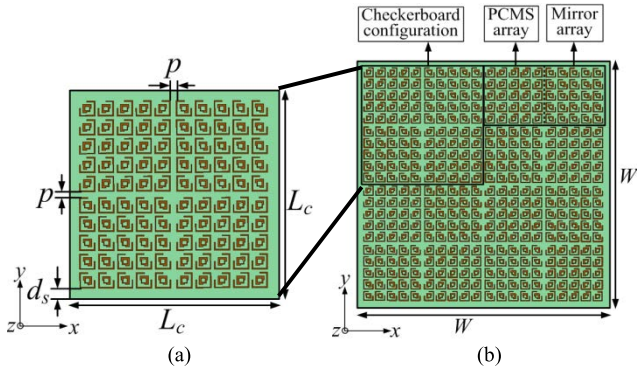

FIGURE 9. Structure of the (a) checkerboard supercell (b) proposed ultrawideband low RCS PCMS. Dimensions are: $L_c = 78$, p = 2.6, $d_s = 4.1$, $W = 156$. All dimensions are in mm.

The parameters 'p' and 'd_s' of the supercell are provided for the ease of the designers and are also selected to obtain ultrawideband RCS reduction. The parameter 'p' measures the gap between each quadrant of the checkerboard structure whereas the parameter 'd_s' measures the distance of the checkerboard surface from the edge of the proposed structure. Changes in the value of 'p' and 'd_s' affect the frequency response of co-polarized monostatic RCS behaviour of a planar copper sheet as depicted in Figure. 10. It is observed from the figure that when the value p is either 1.2 mm or 4 mm and $d_s = 4.8$ mm or 3.4 mm; the RCS reduction bandwidth is less as compared to $p = 2.6$ mm and $d_s = 4.1$ mm. Secondly, the minimum RCS points in both cases do not coincide with the maximum PCR points or the resonant frequency points. Thus, $p = 2.6$ mm and $d_s = 4.1$ mm are chosen as optimized design parameters. In all the above cases the lateral dimensions i.e. $L_c \times L_c$ are maintained constant as 78 mm × 78 mm. The dimensions of the copper sheet are chosen to be the same as the lateral dimensions of the proposed structure (i.e. 78 mm × 78 mm).

Figure. 11 compares the co-polarized monostatic RCS of the large polarization conversion metasurface with that of a planar copper sheet of the same size as the surface for a normal impinging y - polarized plane wave. It is observed that a consistent 10 dB RCS reduction is obtained over a bandwidth of 5.5 – 20.5 GHz with maximum RCS reductions of around -20 dB at 6.8, 9.35, 14.4, and 19.1 GHz.

A study was performed on the choice of the number of MCD square ring resonator-based unit cells to form a quadrant of the supercell. Two important points were considered while choosing the unit cells.

1) The maximum RCS reduction points should almost coincide with the frequency points where PCR value is nearly 100%.

2) There should be a consistent 10 dB RCS reduction covering the entire frequency band of operation.

Keeping this in mind, a simulation study was performed considering the various number of unit cells forming one quadrant of the checkerboard supercell. The outcome is

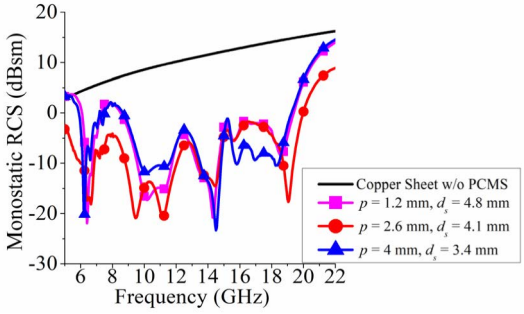

FIGURE 10. Comparison between the simulated co-polarized monostatic RCS of the copper sheet with and without the PCMS array for different values of p, and d_s. The lateral dimensions are fixed.

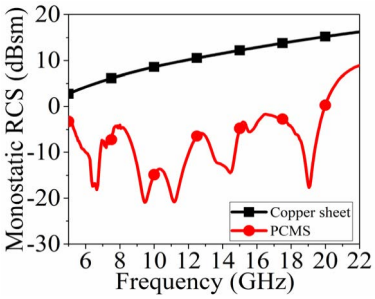

FIGURE 11. Comparison between the simulated co-polarized monostatic RCS of the copper sheet and the PCMS array for a normal incident y-polarized plane wave.

depicted in Figure. 12. It is observed that with only 5 × 5 arrangement of the MCD square ring resonator-based unit cells, the above two criteria are satisfied. The frequency points where maximum RCS reductions are obtained are 6.8, 9.35, 14.4, and 19.1 GHz which nearly coincides with the 100% PCR points of 6.8, 9.3, 14.62, and 19.43 GHz. Other than that, the checkerboard configuration facilitates a consistent 10 dB RCS reduction covering the entire frequency band of operation. As a result, a 5 × 5 configuration is chosen to form a quadrant of the checkerboard structure.

B. RCS REDUCTION OF A CYLINDRICALLY CONFORMAL METALLIC SHEET

There are several microwave and wireless communication applications where surfaces are curved like radomes, ships, aircraft, missiles, and various transmitters. Under these circumstances, the behavior of scattering PCMS surface depends extensively on the curvature of surfaces, as the angle of incidence of the electromagnetic waves changes according to the surface curvature.

In this section, the flat PCMS surface is imported onto the curved cylindrical surfaces of different radii of curvature and their corresponding radar cross sections are determined. They are then compared with a cylindrically curved PEC surface of the same surface area, and the RCS reductions are plotted for each radius of the curved surface.

As discussed previously that the PCBW and PCR values are stable and well preserved for angles of incidence upto

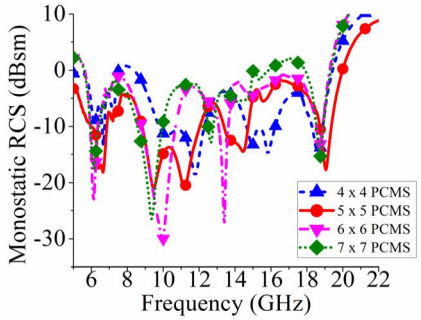

FIGURE 12. Comparison between the simulated co-polarized monostatic RCS of the various configurations of the MCD square ring resonator-based unit cell comprising the PCMS array.

TABLE 3. RCS reduction bandwidths for various central angles of the cylinder under both phi and theta polarizations.

Central Angle, α (°)	RCS Reduction B.W. (%)	
	φ pol	θ pol
0	115	109
30	114.7	108
60	106	83.7
90	69.4	42

±35°, therefore three different radii of curvature of the cylindrical surface with central angles (α) of 30°, 60°, 90° is considered as shown in Figure. 13. We know that the radius of curvature (ROC) (denoted by r here) is inversely proportional to the angle of curvature (denoted by α here). Therefore, for the planar surface, the central angle (α) is 0° and ROC is ∞. For the other three surfaces with central angles of 30°, 60°, and 90°, the radii of curvature are 298, 150, and 99 mm respectively. The RCS of the cylindrically conformal scattering PCMS surface is then compared with the same size of cylindrical PEC surface and the RCS reductions are plotted in Figure. 14 for φ-polarized and θ-polarized normal incident waves respectively.

As seen in Figure. 14, when α is 0° or the surface is flat, the RCS reduction bandwidths are 115% and 109% for φ- and θ-polarizations respectively. For cases of oblique incidence, or when the surface is curved such that electromagnetic wave is incident obliquely, the reflection phase characteristics of the incident wave change for both polarizations, and the RCS reduction performance degrades. Since the performance of the MCD square ring resonator-based unit cell is stable upto ±35° angles of incidence, the RCS reduction bandwidth is almost preserved upto central angles of 70° of the cylindrical PCMS surface and degrades significantly beyond that as evident in Figure. 14.

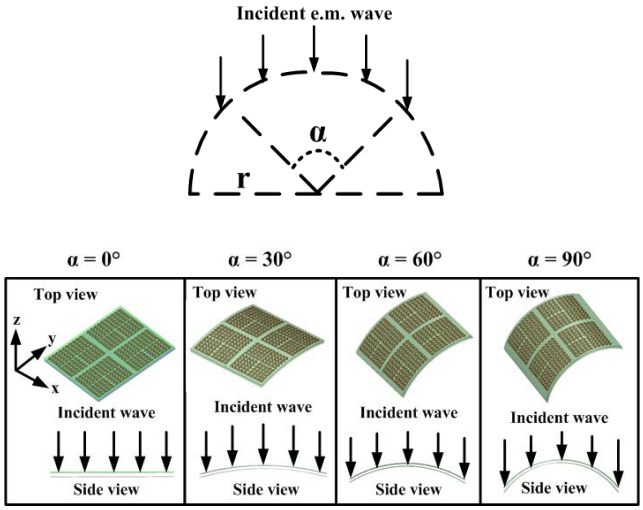

FIGURE 13. Pictorial representation of the incident electromagnetic wave on the cylindrical PCMS surface at central angles (α) of curvature.

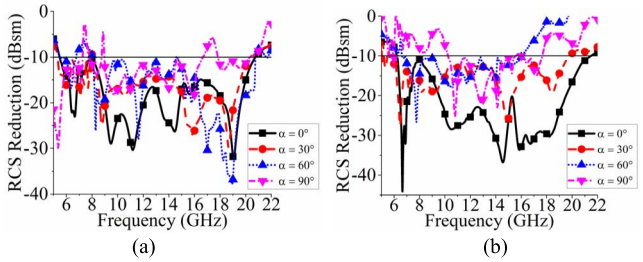

FIGURE 14. Simulated co-polarized monostatic RCS reductions due to the PCMS surface for various central angles (α) under (a) φ-polarized and (b) θ-polarized normal incident waves.

The RCS reduction performance of the flat and curved surfaces for both polarizations has been tabulated in Table 3.

IV. FABRICATION AND EXPERIMENTAL RESULTS

To experimentally investigate the RCS reduction performance of planar and conformal surfaces, the proposed structure is fabricated with 20 × 20 unit cells with lateral dimensions of 156 mm × 156 mm or 3.27 λ_L × 3.27 λ_L (λ_L is the wavelength corresponding to the lowest operating frequency of 6.3 GHz). All the fabricated samples are shown in Figure. 15. The polarization conversion metasurface is realized on a sample of RT/duroid 5880 of thickness 0.508 mm. The metallic ground plane is realized by a copper sheet placed at a distance of 3.5 mm (air gap) from the bottom of the substrate. In order to make the sample mechanically stable, the air gap between the ground plane and the substrate is realized using ROHACELL HF 51 (ε_r = 1.05 and tan δ = 0.0017) foam [34]. As observed in the simulations of Figure. 16, the reflection coefficient is almost unaffected when ROHACELL replaces the air gap, since they are known to have nearly the same permittivity.

Monostatic RCS of the fabricated samples is measured in an anechoic chamber using the method described in [35]

TABLE 4. Comparison of the proposed work with that reported in ref. [31].

Ref.	Substrate thickness, mm	Polarizer thickness, mm	Structure Size (mm × mm × mm) ($\lambda_L \times \lambda_L \times \lambda_L$)	Type of unit cell	10 dB RCS reduction B.W (GHz, %) Flat surface	RCS reduction B.W (%) Curved Surface
[31]	1.52	1.52	200 × 200 × 1.52 ($4.66\lambda_L \times 4.66\lambda_L \times 0.035\lambda_L$), λ_L at 7 GHz	Two different AMCs	7.2 – 8.6 (17%)	10λ ROC: 22.2% (HH pol.), 23.6% (VV pol) 5λ ROC: 25% (HH pol.), 22.2% (VV pol)
This Work	0.508	4	156 × 156 × 4 ($3.27\lambda_L \times 3.27\lambda_L \times 0.08\lambda_L$), λ_L at 6.3 GHz	MCD square ring resonator	5.5 – 20.5 (115%)	For, α = 30°: 114.7 (φ-pol), 108 (θ-pol) For α = 60°: 106 (φ -pol), 83.7 (θ-pol) For α = 90°: 69.4 (φ -pol), 42 (θ-pol)

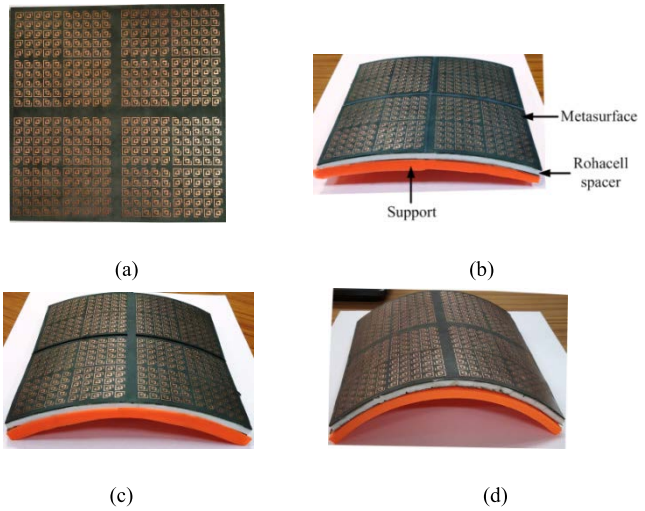

FIGURE 15. Fabricated ultrathin PCMS layer on (a) planar sheet, and mounted on a cylindrical conformal surface with different central angles (b) $\alpha = 30°$ (c) $\alpha = 60°$ (d) $\alpha = 90°$.

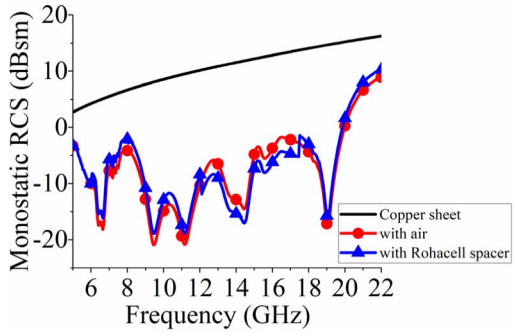

FIGURE 16. Comparison of the frequency response of co-polarized monostatic RCS with air spacer and Rohacell spacer.

(Figure. 17). As observed in the figure, two types of antennas are used in the setup. A transmitting antenna for radiating the incident EM wave onto the periodic structure, and a receiving antenna to measure the scattered fields. In order to cover the measuring frequency range from 5 – 22 GHz, a pair of double ridge horn antennas is used for transmission and reception. The receiving and transmitting horn antenna are placed next to each other tower using a wooden mount. The object under

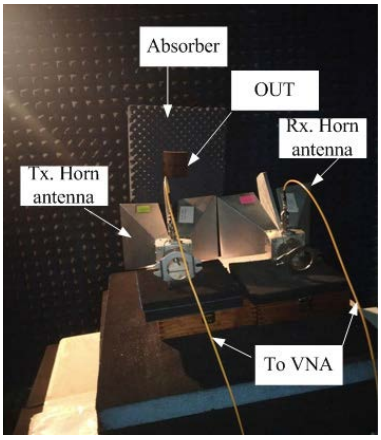

FIGURE 17. RCS measurement setup in an anechoic chamber.

test (OUT) (copper sheet/ fabricated structure) is attached to the absorber surface by means of thin adhesive tapes. To ensure far field of operation, the separation between the antennas and the OUT is maintained at $R = 2D2/\lambda$ (not shown in the figure), where λ is the wavelength corresponding to the lower frequency limit and D is the size of the object under test. With this setup, co-polarized monostatic RCS reductions are measured for both planar as well as conformal surfaces for normal impinging θ- and φ-polarized plane waves.

Figure. 18 shows the comparison between the simulated and measured co-polarized monostatic RCS reductions for normal impinging θ- and φ-polarized plane wave for both planar as well as conformal surfaces with three different central angles with respect to a copper sheet of equal lateral dimensions. It can be seen that the simulated and measured graphs agree well with minor inconsistencies. This is due to the fact that, the impinging waves considered in the simulation are plane waves, while the far-field radiation from the horn antenna is not a standard plane wave. Furthermore, the fabrication tolerance, and other measurement errors like misalignment of surfaces affect the RCS measurements to a certain extent. Discrepancies are more observed for higher values of the central angle, due to tilting of the surfaces to achieve oblique incidence effect.

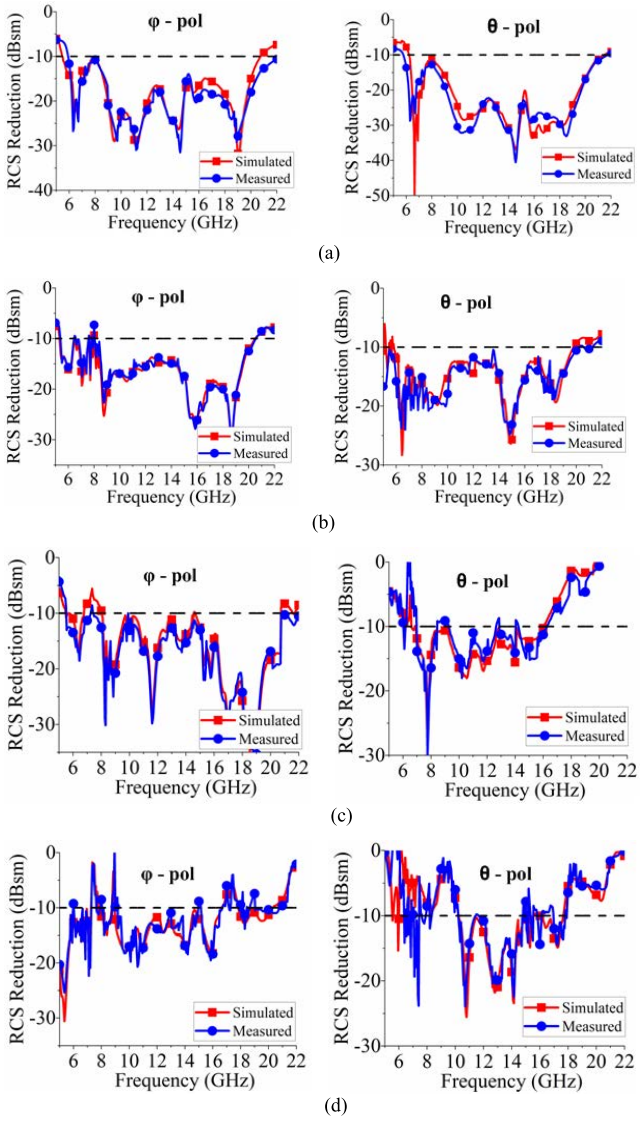

FIGURE 18. Comparison between the simulated and measured co-polarized monostatic RCS reduction for normal incident φ - and θ-polarized waves for (a) flat surface, and conformal surfaces with central angles of (b) $\alpha = 30°$, (c) $\alpha = 60°$, and (d) $\alpha = 90°$.

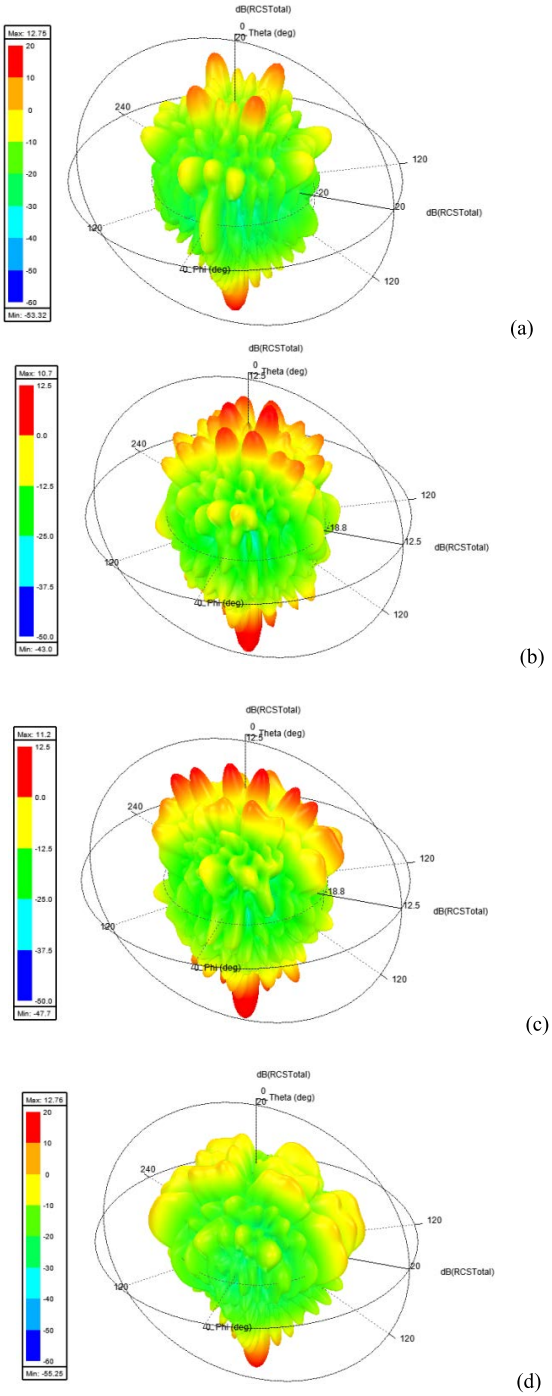

FIGURE 19. 3-D bistatic simulated RCSs-total for φ-polarized normal incident wave for the cases of (a) flat surface at 14.5 GHz and conformal surfaces with central angles of (b) $\alpha = 30°$ at 15.9 GHz, (c) $\alpha = 60°$ at 17 GHz, and (d) $\alpha = 90°$ at 16 GHz.

Limited by the available measurement facility, only simulated results of bistatic RCS of the proposed structure are provided which verify the scattering nature of the surface. Figure. 19 shows the simulated 3-D bistatic RCS of the planar and conformal structures for a normal incident φ – polarized plane wave. It can be observed that the reflected energy is scattered in directions other than the boresight direction for the proposed PCMS surfaces, thereby notably reducing the reflection in the normal direction. This mainly arises due to the phase cancellation of the reflected waves from the PCMS surface as discussed previously. The letter in [31] is the only work that presents a similar concept of wideband RCS reduction of cylindrical surfaces using checkerboard architectures. However, the checkerboard surface in [31] consists of two different AMCs and RCS reduction are not based on the concept polarization conversion. The use of two different AMCs increases the design complexity to some extent. Besides that, only 5 dB RCS reduction is obtained from 7 - 9 GHz for both HH- and VV- polarizations and two different radii of curvature (10λ and λ. The proposed work, however, alleviates the above disadvantages. This work is the first instance where a checkerboard configuration of a single AMC-based PCMS array and its mirror image is used

for RCS reduction of conformal surfaces over an ultrawide bandwidth. Polarization converter based unit cells reduce the structural and design complexity. Besides that, nearly 10 dB co-polarized monostatic RCS reduction is obtained over an ultrawide bandwidth for planar as well as conformal surfaces for both θ- and φ- polarized normal incident waves. Besides that, the ultrathin nature of the substrate makes it suitable for stealth applications involving curved surfaces like radomes, ships, aircraft, missiles, and various transmitters. A comparison between the proposed work and the letter in [31] is given in Table 4 which clearly depicts its advantages.

V. CONCLUSION

A novel polarization conversion based metasurface designed to achieve ultrawideband RCS reduction of planar and conformal surfaces of various radii of curvature is presented in this paper. The PCMS surface comprising of MCD square ring resonator-based unit cells and its mirror image helps to reduce the RCS of a planar copper sheet over a bandwidth of 115% and 109% for θ- and φ-polarized incident waves respectively. Besides that, the designed surface can also reduce the RCS of a curved copper sheet with central angles of 30°, 60°, and 90° over broadband. For all the above cases, a consistent 10 dB co-polarized monostatic RCS reduction is obtained over a wide band of frequencies. The structure is compact and can be applied for stealth applications in military systems operating in X-, Ku-, and parts of C- and K – bands. Measurements conducted agree well with the simulations.

ACKNOWLEDGMENT

The authors would like to thank Vikranth Racherla from the Department of Mechanical Engineering, IIT Kharagpur, Kharagpur, India, for helping in the fabrication of curved PCMS surfaces of the proposed work.

REFERENCES

[1] W. Yang, K.-W. Tam, W.-W. Choi, W. Che, and H. T. Hui, "Polarisation rotation reflective surface based on artificial magnetic conductor and its application," *Electron. Lett.*, vol. 50, no. 21, pp. 1500–1502, Oct. 2014.

[2] Y. Liu, K. Li, Y. Jia, Y. Hao, S. Gong, and Y. J. Guo, "Wideband RCS reduction of a slot array antenna using polarization conversion metasurfaces," *IEEE Trans. Antennas Propag.*, vol. 64, no. 1, pp. 326–331, Jan. 2016.

[3] J. Y. Chin, M. Lu, and T. J. Cui, "Metamaterial polarizers by electric-field-coupled resonators," *Appl. Phys. Lett.*, vol. 93, no. 25, 2008, Art. no. 251903.

[4] X. Xiong, S.-C. Jiang, Y.-S. Hu, Y.-H. Hu, Z.-H. Wang, R.-W. Peng, and M. Wang, "Control the polarization state of light with symmetry-broken metallic metastructures," *Ann. Phys.*, vol. 358, pp. 129–158, Jul. 2014.

[5] Y. Zhao and A. Alù, "Manipulating light polarization with ultrathin plasmonic metasurfaces," *Phys. Rev. B, Condens. Matter*, vol. 84, no. 20, Nov. 2011, Art. no. 205428.

[6] D. R. Smith, W. J. Padilla, D. C. Vier, S. C. Nemat-Nasser, and S. Schultz, "Composite medium with simultaneously negative permeability and permittivity," *Phys. Rev. Lett.*, vol. 84, pp. 4184–4187, May 2000.

[7] C. L. Holloway, E. F. Kuester, J. A. Gordon, J. O'Hara, J. Booth, and D. R. Smith, "An overview of the theory and applications of metasurfaces: The two-dimensional equivalents of metamaterials," *IEEE Antenn. Propag. Mag.*, vol. 54, no. 4, pp. 10–35, Apr. 2012.

[8] H.-T. Chen, A. J. Taylor, and N. Yu, "A review of metasurfaces: Physics and applications," *Rep. Prog. Phys.*, vol. 79, no. 7, Jul. 2016, Art. no. 076401.

[9] J. Chatterjee, A. Mohan, and V. Dixit, "Broadband circularly polarized H-shaped patch antenna using reactive impedance surface," *IEEE Antennas Wireless Propag. Lett.*, vol. 17, no. 4, pp. 625–628, Apr. 2018.

[10] D. Kundu, A. Mohan, and A. Chakrabarty, "Ultrathin high-efficiency X-band reflective polarization converter using sunken double arrowhead metasurface," in *Proc. Asia–Pacific Microw. Conf. (APMC)*, New Delhi, India, Dec. 2016, pp. 1–4.

[11] Z. Lei and T. Yang, "Converting state of polarization with a miniaturized metasurface device," *IEEE Photon. Technol. Lett.*, vol. 29, no. 7, pp. 615–618, Apr. 1, 2017.

[12] T. Cai, G.-M. Wang, X.-L. Fu, J.-G. Liang, and Y.-Q. Zhuang, "High-efficiency metasurface with polarization-dependent transmission and reflection properties for both reflectarray and transmitarray," *IEEE Trans. Antennas Propag.*, vol. 66, no. 6, pp. 3219–3224, Jun. 2018.

[13] X. Gao, X. Han, W.-P. Cao, H. O. Li, H. F. Ma, and T. J. Cui, "Ultrawideband and high-efficiency linear polarization converter based on double V-shaped metasurface," *IEEE Trans. Antennas Propag.*, vol. 63, no. 8, pp. 3522–3530, Aug. 2015.

[14] N. Yu, P. Genevet, M. A. Kats, F. Aieta, J.-P. Tetienne, F. Capasso, and Z. Gaburro, "Light propagation with phase discontinuities: Generalized laws of reflection and refraction," *Science*, vol. 334, no. 6054, pp. 333–337, Oct. 2011.

[15] Y. Jia, Y. Liu, Y. J. Guo, K. Li, and S.-X. Gong, "Broadband polarization rotation reflective surfaces and their applications to RCS reduction," *IEEE Trans. Antennas Propag.*, vol. 64, no. 1, pp. 179–188, Jan. 2016.

[16] W. Yang, K. W. Tam, W. W. Choi, W. Che, and H. T. Hui, "Novel polarization rotation technique based on an artificial magnetic conductor and its application in a low-profile circular polarization antenna," *IEEE Trans. Antennas Propag.*, vol. 62, no. 12, pp. 6206–6216, Dec. 2014.

[17] H. Chen, H. Ma, J. Wang, S. Qu, Y. Pang, M. Yan, and Y. Li, "Ultra-wideband transparent 90° polarization conversion metasurfaces," *Appl. Phys. A, Solids Surf.*, vol. 122, no. 4, p. 463, Apr. 2016.

[18] Y.-F. Cheng, X. Ding, and W. Shao, "A novel checkerboard AMC surface for X-, Ku-and K-band RCS reduction," in *Proc. IEEE Int. Symp. Antennas Propag. USNC/URSI Nat. Radio Sci. Meeting*, San Diego, CA, USA, Jul. 2017, pp. 1927–1928.

[19] F. Ding, Z. Wang, S. He, V. M. Shalaev, and A. V. Kildishev, "Broadband high-efficiency half-wave plate: A supercell-based plasmonic metasurface approach," *ACS Nano.*, vol. 9, no. 4, pp. 4111–4119, Mar. 2015.

[20] Z. Wei, Y. Cao, Y. Fan, X. Yu, and H. Li, "Broadband polarization transformation via enhanced asymmetric transmission through arrays of twisted complementary split-ring resonators," *Appl. Phys. Lett.*, vol. 99, pp. 221907-1–221907-3, Nov. 2011.

[21] H.-Y. Chen, "Broadband perfect polarization conversion metasurfaces," *Chin. Phys. B*, vol. 24, no. 1, 2015, Art. no. 014201.

[22] M. Feng, J. Wang, H. Ma, W. Mo, H. Ye, and S. Qu, "Broadband polarization rotator based on multi-order plasmon resonances and high impedance surfaces," *J. Appl. Phys.*, vol. 114, Aug. 2013, Art. no. 074508.

[23] Y. Jia, Y. Liu, W. Zhang, and S. Gong, "Ultra-wideband and high-efficiency polarization rotator based on metasurface," *Appl. Phys. Lett.*, vol. 109, no. 5, Aug. 2016, Art. no. 051901.

[24] B. Lin, B. Wang, W. Meng, X. Da, W. Li, Y. Fang, and Z. Zhu, "Dual-band high-efficiency polarization converter using an anisotropic metasurface," *J. Appl. Phys.*, vol. 119, no. 18, May 2016, Art. no. 183103.

[25] A. Y. Modi, C. A. Balanis, C. R. Birtcher, and H. N. Shaman, "Novel design of ultrabroadband radar cross section reduction surfaces using artificial magnetic conductors," *IEEE Trans. Antennas Propag.*, vol. 65, no. 10, pp. 5406–5417, Oct. 2017.

[26] M. I. Khan, Q. Fraz, and F. A. Tahir, "Ultra-wideband cross polarization conversion metasurface insensitive to incidence angle," *J. Appl. Phys.*, vol. 121, no. 4, Jan. 2017, Art. no. 045103.

[27] X. Huang, H. Yang, D. Zhang, and Y. Luo, "Ultrathin dual-band metasurface polarization converter," *IEEE Trans. Antennas Propag.*, vol. 67, no. 7, pp. 4636–4641, Jul. 2019.

[28] L. Zhang and T. Dong, "Low RCS and high-gain CP microstrip antenna using SA-MS," *Electron. Lett.*, vol. 53, no. 6, pp. 375–376, Mar. 2017.

[29] Y. Jia, Y. Liu, Y. J. Guo, K. Li, and S. Gong, "A dual-patch polarization rotation reflective surface and its application to ultra-wideband RCS reduction," *IEEE Trans. Antennas Propag.*, vol. 65, no. 6, pp. 3291–3295, Jun. 2017.

[30] Y.-F. Cheng, X. Ding, and W. Shao, "A novel checkerboard AMC surface for band RCS reduction," in *Proc. IEEE Int. Symp. Antennas Propag. USNC/URSI Nat. Radio Sci. Meeting*, San Diego, CA, USA, Jul. 2017, pp. 1927–1928.

[31] W. Chen, C. A. Balanis, C. R. Birtcher, and A. Y. Modi, "Cylindrically curved checkerboard surfaces for radar cross-section reduction," *IEEE Antennas Wireless Propag. Lett.*, vol. 17, no. 2, pp. 343–346, Feb. 2018.
[32] D. Yoharaaj, R. S. Azmir, and A. Ismail, "A new approach for bandwidth enhancement technique in microstrip antenna for wireless applications," in *Proc. Int. RF Microw. Conf.*, Putrajaya, Malaysia, Sep. 2006, pp. 205–209.
[33] N. T. Tung, V. T. T. Thuy, J. W. Park, J. Y. Rhee, and Y. Lee, "Left-handed transmission in a simple cut-wire pair structure," *J. Appl. Phys.*, vol. 107, no. 2, Jan. 2010, Art. no. 023530.
[34] Evonik Industries. (Jan. 2020). *Rohacell Dielectric Properties*. [Online]. Available: https://www.rohacell.com/en/products-services/rohacell-hf
[35] W. Pan, C. Huang, P. Chen, X. Ma, C. Hu, and X. Luo, "A low-RCS and high-gain partially reflecting surface antenna," *IEEE Trans. Antennas Propag.*, vol. 62, no. 2, pp. 945–949, Feb. 2014.

JOYSMITA CHATTERJEE (Graduate Student Member, IEEE) received the B.Tech. degree in electronics and communication engineering from the West Bengal University of Technology, West Bengal, India, in 2009, and the M.Tech. degree from the National Institute of Technology (NIT) Durgapur, West Bengal, in 2012. She is currently pursuing the Ph.D. degree with the Indian Institute of Technology (IIT) Kharagpur, West Bengal.

She joined IIT Kharagpur, in 2016. She has worked as an Assistant Professor in various private engineering universities and colleges, from 2012 to 2016, such as KIIT University, Bhubaneswar, Odisha, India, the ABES Engineering College, Ghaziabad, India, and the Inderprastha Engineering College, Ghaziabad, India, where she was involved in teaching and other academic and research activities. Her research interests include metamaterial and metasurface-based planar antennas, reconfigurable antennas, MIMO antenna, and for various wireless communication applications.

AKHILESH MOHAN (Member, IEEE) received the B.Tech. degree in electronics engineering from the Kamla Nehru Institute of Technology, Sultanpur, India, in 2002, and the M.Tech. and Ph.D. degrees in microwave engineering from the Indian Institute of Technology Kanpur, Uttar Pradesh, India, in 2004 and 2009, respectively.

From 2009 to 2010, he worked as a Scientist with the Applications Center, Indian Space Research Organization, Ahmedabad, India. From 2010 to 2021, he was a Faculty Member with the Department of Electrical Engineering, Indian Institute of Technology Jodhpur, Rajasthan, India, and the Indian Institute of Technology Kharagpur, West Bengal, India, where he was involved in teaching and research activities. Since February 2021, he has been a Faculty Member with the Department of Electronics and Communication Engineering, Indian Institute of Technology Roorkee, Uttarakhand, India. He has authored or coauthored more than 120 peer-reviewed international journals and conference papers. His research interests include the design of microwave filters and planar antennas for wireless communication systems.

VIVEK DIXIT (Member, IEEE) received the B.Tech. degree in electrical engineering from IIT Delhi, New Delhi, India, and the Ph.D. degree from the Department of Electrical and Computer Engineering, National University of Singapore, Singapore.

He is currently working as an Assistant Professor with the Department of Electronics and Electrical Communication Engineering, IIT Kharagpur, Kharagpur, India. His research interests include semiconductor devices and simulation, RF and microwave circuits, optoelectronics and metamaterials, and silicon photonics.